J Mol Model (2014) 20:2470
DOI 10.1007/s00894-014-2470-7

ORIGINAL PAPER

Molecular modeling and simulation of the human eNOS reductase domain, an enzyme involved in the release of vascular nitric oxide

N. T. Devika · Prakash Amresh · Md. Imtiyaz Hassan · B. M. Jaffar Ali

Received: 19 January 2014 / Accepted: 14 September 2014 / Published online: 7 October 2014

Abstract Homology modeling of the reductase domain of endothelial nitric oxide synthase (eNOS), which regulates the catalytic activity of eNOS, and molecular dynamics studies focusing especially on the serine residues S615, S633, and S1177 were performed. MD analysis of this structure revealed that S633 is highly flexible and accessible to solvent molecules, while S1177 becomes highly flexible when S633 is phosphorylated. The presence of intramolecular interactions between S1177 among the major serine residues underscores its structural importance to the efficient synthesis of nitric oxide in endothelium. In order to evaluate the appropriateness of phosphomimetic (for phosphorylation) and phosphomutant (for dephosphorylation) eNOSs for use as experimental model systems, the structural dynamics and conformational changes in phosphomimetic (S615D, S633D, S1177D) and phosphomutant (S615A, S633A, S1177A) eNOSs were investigated. Phosphomimetic and phosphomutant eNOSs portrayed S633 as a modulator of S1177, whereas such correlations could not be observed in native and phosphorylated eNOSs. Computational analysis of the docked complex revealed that phosphorylated pS1177 and pS615 have high affinity for Akt (one of the key kinases in the eNOS activation pathway), with a significant number of hydrogen bonds and salt bridges observed between these residues and Akt . This work therefore provides evidence of the subtle structural changes that occur within the reductase domain which contribute to the stability–flexibility–activity relationship of eNOS. Such subtle changes are of great importance in the context of regulated nitric oxide release by different phosphorylated forms of eNOS and the need to account for the existence of subtle differences between real proteins and experimental model systems.

Keywords Endothelial nitric oxide synthase · Molecular dynamics · Phosphorylation · Phosphomimetic · Phosphomutant · Signaling protein · Nitric oxide

Introduction

Numerous cardiovascular functions are performed by nitric oxide (NO), a ubiquitous inter- and intracellular signaling molecule [1, 2]. NO is synthesized in diverse mammalian tissues by three homologous isoforms of nitric oxide synthase (NOS)—neuronal NOS (nNOS/NOS1) [3], inducible NOS (iNOS/NOS2) [4], and endothelial NOS (eNOS/NOS3)—encoded by distinct genes [5]. These three mammalian isoforms share 50–60 % sequence identity but differ in size, intracellular location, regulation, and catalytic and inhibitory properties [6]. Among the NOS isoforms, eNOS is the predominant source of bioavailable vascular NO and the fundamental determinant of vascular homeostasis, which regulates systemic blood pressure, angiogenesis, vascular remodeling,

Electronic supplementary material The online version of this article (doi:10.1007/s00894-014-2470-7) contains supplementary material, which is available to authorized users.

N. T. Devika
AU-KBC Research Centre, Madras Institute of Technology, Anna University, Chrompet, Chennai 600 044, Tamil Nadu, India
e-mail: ntdevika@gmail.com

P. Amresh · M. Hassan
Centre for Interdisciplinary Research in Basic Sciences, Jamia Millia Islamia, Jamia Nagar, New Delhi 11025, India

P. Amresh
e-mail: prakashamresh@gmail.com

M. Hassan
e-mail: mihassan@jmi.ac.in

N. T. Devika · B. M. J. Ali (✉)
Centre for Green Energy Technology, Pondicherry University, Kalapet, Puducherry 605 014, India
e-mail: jaffarali.bm@gmail.com

and smooth muscle relaxation [7, 8]. It possesses a common bidomain structure, with a N-terminal oxygenase domain containing the heme core and binding sites for L-arginine and tetrahydrobiopterin as well as a C-terminal reductase domain harboring binding sites for FMN, FAD, and NADPH [9], interlinked by calmodulin-binding sites. The primary function of the reductase domain is to efficiently transfer electrons from NADPH via two prosthetic groups, FAD and FMN, to the heme center present in the oxygenase domain, thus allowing the heme to be reduced. The reduced heme can then produce NO from the NOS substrates oxygen and L-arginine [10].

Further, the distinct mechanisms that regulate eNOS activity include subcellular localization, post-translational modifications such as phosphorylation and dephosphorylation, and associations with other regulatory molecules [11, 12]. The serine/threonine phosphorylation sites identified within the reductase domain play a key role in the regulation of the catalytic activity of eNOS [13]. Multiple signaling protein kinases—including protein kinase B (Akt/PKB), protein kinase A (PKA), protein kinase G, AMP activated protein kinase, and CaM kinase II—regulate eNOS by phosphorylating serine residues (S615, S633, and S1177) localized in the reductase domain stimulated by a variety of humoral, mechanical, and pharmacological stimuli [14, 15].

The phosphorylation of eNOS at S1177 has been extensively characterized and shown to be crucial for maximizing the enzymatic activity of eNOS [16, 17] in response to a growing list of stimuli, including shear stress [18] and humoral factors such as bradykinin [19] and insulin [20]. Similarly, phosphorylation at S615 and S633, which are located in the autoinhibitory loop present within the FMN-binding domain, are known to be stimulated by VEGF, ATP, and bradykinin [21]. There is also substantial evidence that shear stress stimulates phosphorylation at S633 without the need for an increase in intracellular Ca^{2+} [22, 23].

The X-ray crystal structures of the eNOS oxygenase domain and nNOS reductase domain have already been solved [24, 25], but the structure of the human $eNOS_{red}$ domain remains to be determined. This is needed to elucidate the molecular mechanism of phosphorylation and enzymatic regulation. In the work reported in the present paper, we modeled the three-dimensional structure of $eNOS_{red}$ and carried out extensive molecular dynamics studies to determine possible structural modulations and regulation associated with the phosphorylation of important serine residues.

Experimental approaches to discern the role of multisite phosphorylation and dephosphorylation of eNOS in the regulation and release of NO downstream utilize phosphomimetic and phosphomutant eNOS constructs to achieve stable phosphorylated and dephosphorylated eNOS proteins [26]. In order to relate the molecular dynamic simulation data to experimental results, structural modeling and molecular dynamics study was carried out for native, phosphorylated (pS615, pS633, and pS1177), phosphomimetic (S615D, S633D, and S1177D), and phosphomutant (S615A, S633A and S1177A) eNOSs. We analyzed the structural stabilities and dynamic properties of native, phosphorylated, phosphomimetic, and phosphomutant eNOSs with MD simulations and compared the results with the experimental findings reported in the literature. In addition, we examined the inter- and intramolecular interactions of the distinct forms of eNOS with Akt, which permitted a better understanding of the binding association of eNOS with Akt and the regulation of eNOS.

Materials and methods

Homology modeling

The eNOS protein sequence of *Homo sapiens* (P29474) was retrieved from the UniProtKB (http://www.uniprot.org) database. The human eNOS contains a sequence of 1203 amino acids, and 678 residues from 511 to 1188 in the reductase domain were considered for the current study. A homology-modeled structure was generated by performing several steps of sequence alignment and structural modeling using Modeller [27]. The numbering scheme used for the amino acids considered in this study was based on the full-length sequence. A Protein BLAST (BLASTP) search was carried against PDB to identify the suitable template. Three proteins (PDB ID: 1TLL, 1F20, and 3HR4) with structural identities of 56 %, 55 %, and 40 % were identified as possible templates. Multiple templates were selected to increase the accuracy of the model. The SALIGN command of Modeller was employed for multiple structure alignment of template structures. SALIGN performs a pairwise alignment by dynamic programming optimization using a scoring function that is dependent on the sequence and structural features. The input script of Modeller reads all of these template structures to generate a three-dimensional model structure. A total of ten models were generated for eNOS and ranked according to discrete optimized protein energy (DOPE) score. The correctness and stereochemical quality of the predicted models were analyzed with Procheck [28], Verify3D [29], and Errat [30].

Molecular dynamics simulation

All simulations were performed with the GROMACS (v4.5.5) program [31] using the GROMOS96 43a1 force field. Phosphorylation at major serine residues, namely S615, S633, and S1177, was carried with the Vienna-PTM utility, a toolkit used to explore post-translational modifications using MD simulations [32]. Mutation was performed on the serine

residues to aspartate (S615D, S633D, and S1177D, representing the phosphomimetic eNOS) and to alanine (S615A, S633A, and S1177A, representing the phosphomutant eNOS) using the web server Whatif (http://swift.cmbi.ru.nl/whatif/). The coordinates of these ten proteins (native, pS615, pS633, pS1177, S615D, S633D, S1177D, S615A, S633A, and S1177A) were energy-minimized and subjected to MD simulation with the aim of evaluating the post-translational changes and structural stability of the human $eNOS_{red}$ domain. The native and phosphorylated protein structures were solvated in a dodecahedral box of spc216 water molecules, and the solvated system was neutralized by adding one Cl^- ion. A total of four Na^{2+} ions were added to the phosphomimetic or phosphomutant protein system. Further, the solvated system was first minimized using 1000 steepest-descent steps, and a conjugate gradient algorithm was then applied to remove bad contacts, with a convergence criterion of 0.01 kJ mol^{-1} nm^{-1}. All of the heavy atoms were restrained (limited to their starting positions) while the water molecules were allowed to relax around the structure. This molecular system was then equilibrated in two steps: first, a simulation using the NVT ensemble with no pressure coupling and the Berendson thermostat was performed; second, a simulation using the NPT ensemble with a pressure of 1.0 bar (P) and the Parrinello–Rahman method was carried out [33]. During both steps, the constraints were maintained on all of the bonds (including heavy H atoms) using a leapfrog integrator [34] and periodic boundary conditions. Finally, the system was submitted to a 40 ns simulation with a time step of 2 fs at a temperature of 300 K and a pressure of 1 bar for the native and phosphorylated proteins, and a 10 ns simulation for the phosphomimetic and phosphomutant. Prior to this, MD simulation was also performed on the native eNOS protein for 10 ns (Fig. S1 of the Electronic supplementary material, ESM) in order to ascertain the equivalence to the 40 ns simulation data (Fig. 3a), and the equivalence was found to be satisfactory. Hence, short-duration 10 ns MD simulations were carried out on the phosphomutant and phosphomimetic structures. The particle mesh Ewald (PME) method was used to compute the long-range electrostatic interactions, and a 1.4 nm cutoff was employed for van der Waals interactions, whereas a 1.0 nm cutoff for Coulomb interactions was adopted in the simulation. The equation of motion was integrated using the leapfrog algorithm with 2.0 fs time steps and the trajectory was saved every 1000 steps (2 ps). The tools built into GROMACS returned the root mean square deviation (RMSD) and the root mean square fluctuation (RMSF), the values of which were tracked to ensure the system remained in equilibrium. The protein was visualized using PyMOL. The solvent accessibility of the amino acids was determined using ASAView (http://www.abren.net/asaview/) [35].

Protein–protein docking

The HADDOCK [36] protocol was employed to dock the distinct forms of eNOS with Akt. The CPORT tool in the HADDOCK server uses a combination of six different interface prediction techniques to predict the active and passive residues required to perform docking studies [37]. HADDOCK scoring was performed according to the weighted sum (the HADDOCK score) of various energy terms, including the van der Waals energy, electrostatic energy, distance restraint energy, binding energy, desolvation energy, and buried surface area. The representative structure was chosen based on the lowest RMSD.

Molecular interactions

The web server ESBRI (http://bioinformatica.isa.cnr.it/ESBRI/introduction.html) [38] was used to check the protein structure for the presence of salt bridges between positively or negatively charged residues based on the atomic coordinates, with the threshold distance fixed at 4 Å. The Protein Interaction Calculator (PIC) server (http://pic.mbu.iisc.ernet.in/) [39] was used to determine inter- and intramolecular hydrogen bonds in the protein structure.

Results

Molecular modeling

The three-dimensional structure of the human $eNOS_{red}$ domain was predicted in order to increase our molecular-level understanding of its function in eNOS activation pathways. The refined model had 89.30 % of the residues in the allowed region of the Ramachandran plot (Fig. 1). The *G* factor was impressive, with a score of −0.38, indicating that the generated model satisfied the stereochemical criteria (i.e., covalent and overall bond or angle distances). All-atom superposition of the predicted $eNOS_{red}$ domain model yielded very similar RMSDs of 0.69 Å, 0.64 Å, and 0.7 Å with the selected templates PDB ID: 1TLL, 1 F20, and 3HR4, respectively, indicating fairly good overlap between structures. Verify3D analysis of the generated model yielded 94.85 % of the residues with an average score of > 0.2, suggesting a fairly good model. Further, an ERRAT score of 60.57 % was obtained for the model. The energy-minimized structure of the human $eNOS_{red}$ domain is shown in Fig. 2.

The main-chain RMSD for the native structure of $eNOS_{red}$ was plotted as a time-dependent function, as shown in Fig. 3a. During the course of the simulation, the modeled protein structure stabilized to a value of 3.8 Å in 10 ns and remained approximately this value until the end of the 40 ns simulation.

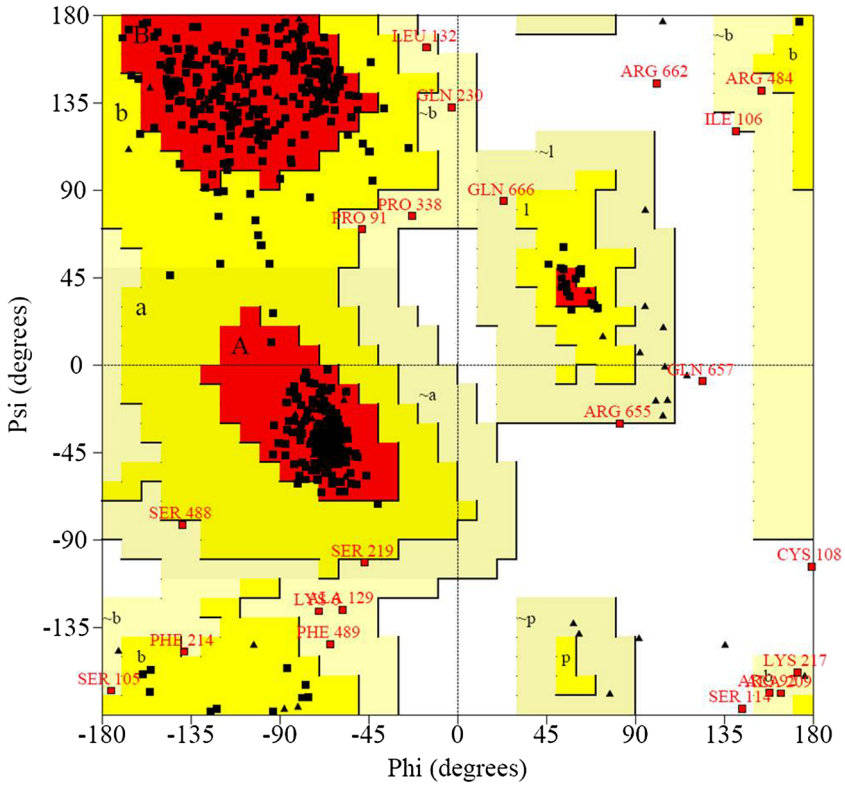

Fig. 1 Ramachandran plot of the human $eNOS_{red}$ domain as derived from homology modeling

The residues in the loop region that are rich in glycine, i.e., residues 835–840 (Gly, Ser, Pro, Gly, Gly, Pro), showed the greatest fluctuations, with a mean of 4 Å calculated for the entire set of 678 residues. In addition, the flavodoxin-binding region corresponding to residues 594–606 showed a mean flexibility of 3 Å. Further, it was noted that residues K631, E632, A719, and F724 in the loop region also showed a relatively high degree of fluctuation, 2.8 Å. The RMSF plot shown in Fig. 4a clearly shows that S633 has the greatest flexibility among the phosphorylated residues, with a deviation of around 3.4 Å as compared to around 2 Å and 1.5 Å for S615 and S1177, respectively.

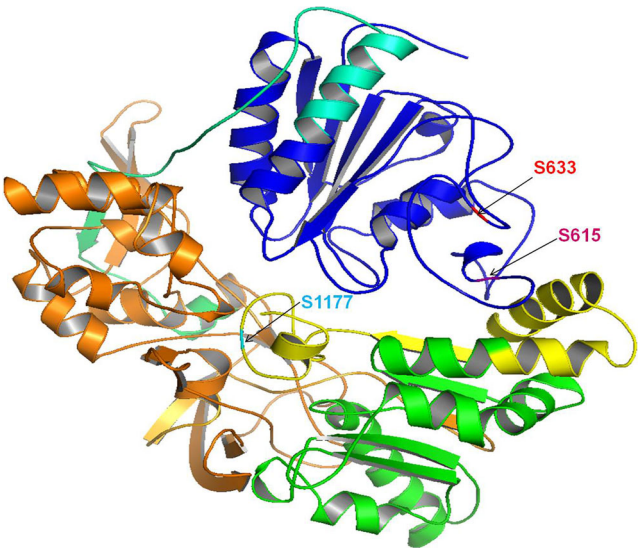

Fig. 2 3D structure of the human $eNOS_{red}$ domain, generated using Modeller. Different binding domain regions have been identified and are color-coded: *blue* flavodoxin, *orange* FAD, *green* NADPH

Molecular dynamics of phosphorylated $eNOS_{red}$

Molecular dynamic studies of phosphorylated $eNOS_{red}$ showed that the RMSDs of pS633 and pS1177 converged around 5 Å (Fig. 3b, c), and around 4.5 Å for pS615 eNOS (Fig. 3d), within 10 ns. The RMSF data show that the residues present in the loop regions exhibit a great deal of movement, and the N- and C-terminal regions are also prone to significant fluctuations (Fig. 4a–d). Upon analyzing the phosphorylated residues, S633 was found to undergo the largest fluctuations, with an RMSF of 3.8 Å observed in its phosphorylated state (Fig. 4c). In the case of S615, the greatest RMSF (2 Å) was observed upon phosphorylation at S633 (Fig. 4c). On the contrary, S1177 showed only marginal fluctuations when compared to the other phosphorylated residues. In a comparison with the native eNOS, all of the phosphorylated eNOSs were found to exhibit high flexibilities (Fig. 4a–d). Specifically, the residues 560–562, 624–634, 712–714, 731–732, 771–773, 965–968, 1001–1005, and 1133–1140 showed

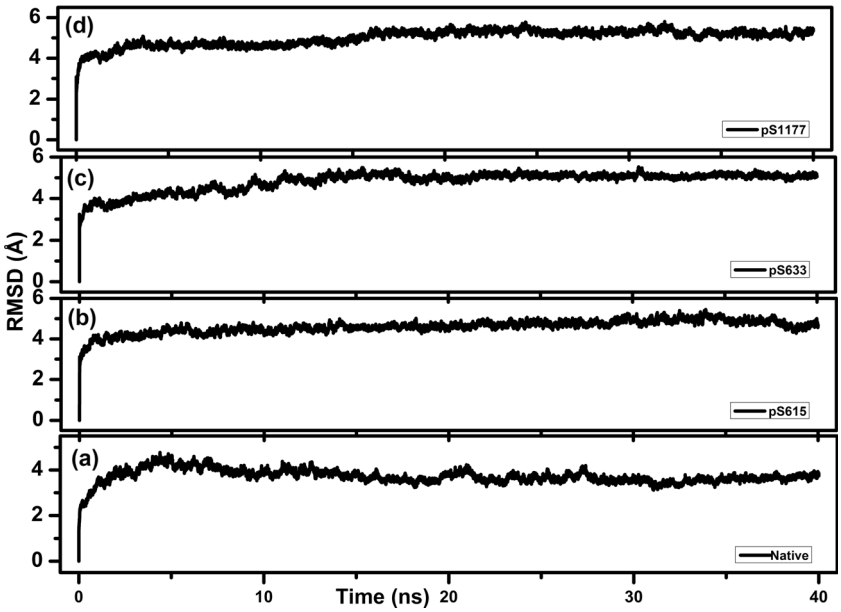

Fig. 3a– RMSD profiles for eNOS and phosphorylated systems: **a** native, **b** pS615, **c** pS633, **d** pS1177

greater flexibility with respect to pS633 than to native and other phosphorylated eNOSs.

Molecular dynamics of phosphomimetic $eNOS_{red}$

In order to mimic the phosphorylated protein residues used in experimental assays, they were substituted with aspartate [13, 16]. However, structurally phosphorylated serine (S) and aspartate (D) should present different conformational states. In the eNOS activation pathways, since multiple phosphorylation sites contribute to the subtle differential regulation of eNOS, it is reasonable to determine and differentiate the effects of these distinct structural features. To achieve this, MD simulations were carried out on the major serine residues, namely S615, S633, and S1177, which had been substituted with aspartate (D), i.e., phosphomimetic modification. The S633D and S1177D eNOSs displayed an increase in RMSD to ~3.5 Å (Fig. 5b, c), while S615D reached a steady value of ~3.3 Å (Fig. 5a). The highly flexible region of the native eNOS (residues 835–840) exhibited similar levels of deviation in all of the phosphomimetic eNOSs. The calculated mean RMSF values of the highly flexible region (residues 835–840) were 7.4 Å, 6.8 Å, and 4.4 Å, respectively, for S615D, S633D, and S1177D (Fig. 6a–c). Among the three phosphorylation

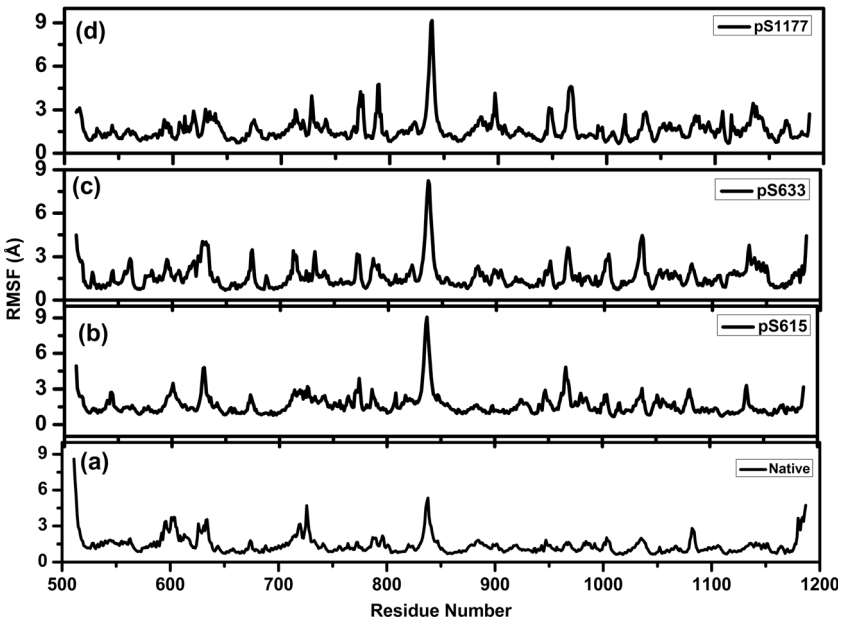

Fig. 4 RMSF plots for eNOS and phosphorylated systems: **a** native, **b** pS615, **c** pS633, **d** pS1177

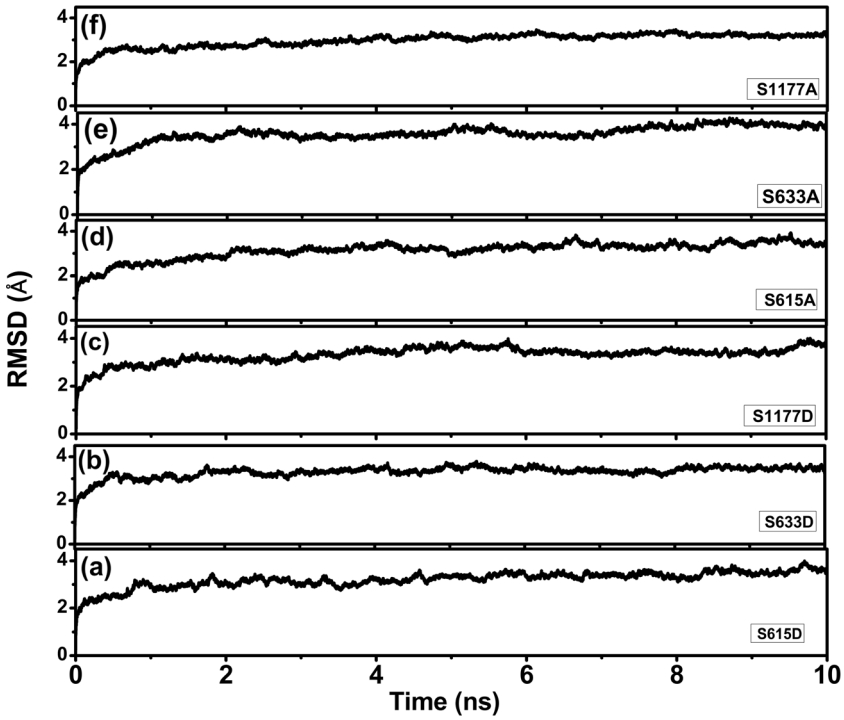

Fig. 5a–f Time-dependent RMSD plot for eNOS in different states: **a–c** phosphomimetic S615D, S633D, S1177D; **d–f** phosphomutant S615A, S633A, S1177A

residues that are pertinent to this study, S633 was found to be the most flexible. It exhibited a maximum fluctuation of 3.8 Å upon S1177D substitution (Fig. 6c). For S615, a fluctuation of 1.8 Å was observed upon S633D substitution (Fig. 6b), whereas S1177 represented a maximum fluctuation of 1.2 Å upon S615D substitution (Fig. 6a).

Molecular dynamics of phosphomutant $eNOS_{red}$

In order to maintain the dephosphorylated eNOS state in an experimental dissection of pathways, it is customary to mutate serine to alanine [16]. However, eNOS-Ser (dephosphorylated) and eNOS-Ala are structurally different moieties. Therefore, in the present study, MD simulations were performed to differentiate the structural features of eNOS phosphomutants, i.e., S615A, S633A, and S1177A. Analysis of the phosphomutant eNOS revealed that S633A had a larger RMSD, ~3.5 Å (Fig. 5e), than S615A and S1177A, both of which had an RMSD of 3 Å (Fig. 5d, f). RMSF analysis of the highly flexible glycine-rich region (835–840) and its adjacent residues, namely 789–790, 967–968, and 1134–1135, revealed a maximum RMSF of 8 Å for the S1177A mutation. Notably, residues K631, Q632, and F724 exhibited high fluctuations of around 4 Å with respect to S615A. The phosphorylation residue S615 showed a reduced RMSF of 1.2 Å when S633 was dephosphorylated (Fig. 6e), whereas a higher RMSF of 4.3 Å was observed for S633 upon the phosphomutation of S615 (Fig. 6d). Similarly, the major phosphorylation residue S1177 showed a flexibility of 1.3 Å upon S633 phosphomutation (Fig. 6e).

Solvent accessibility analyses of the native, phosphorylated, phosphomimetic, and phosphomutant eNOSs were carried out. We found that S633 was the most accessible of the residues involved in phosphorylation (Fig. S2 of the ESM). S633 was most accessible in its phosphorylated state, whereas it was least accessible upon S615 phosphorylation. The experimental evidence indicated that the location of the S633 residue in the FMN-binding domain resulted in maximum eNOS activity [40] upon the substitution of S633D—an effect that is comparable to S1177-mediated enzymatic activity. However other residues, namely S615 and S1177, were less accessible.

Intramolecular interactions

The H-bond interactions and possible perturbations to the structures of all of the proteins discussed above were analyzed to elucidate changes in the contacts and conformations of the phosphorylated residues. The intramolecular hydrogen bonds exhibited by pS1177 and S1177D are listed in Table 1. The contact data for other residues are summarized in Table S1 of the ESM. Analysis of the hydrogen bonds in phosphorylated eNOSs revealed that pS633 is capable of forming the greatest number of hydrogen bonds (Table S1 of the ESM). In contrast, the pS1177 eNOS showed the fewest H-bonds (Table 1). Interestingly, the S1177D eNOS exhibited more intramolecular H-bonds than the native and phosphorylated eNOSs (Table 1). This observed stability of the S1177D eNOS supports the reported experimental finding that S1177D is

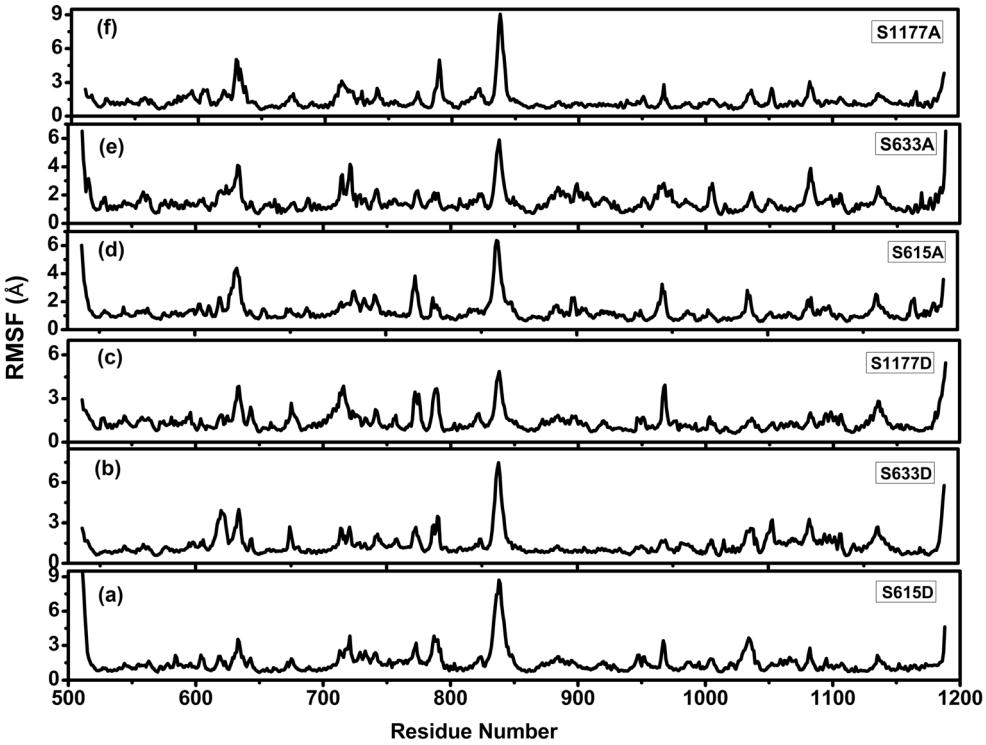

Fig. 6a–f Average RMS fluctuation per residue plot for eNOS in different states: **a–c** phosphomimetic S615D, S633D, S1177D; **d–f** phosphomutant S615A, S633A, S1177A

correlated with increased enzymatic activity and NO production in endothelial cells [41, 42].

Similarly, the salt bridges between the residues were analyzed. Table S2 of the ESM gives more details. The highly flexible pS633 also formed two complex salt bridges: R1000 with D578 of the flavodoxin-binding region, and R1165 with D1116 of the NAD-binding region. In the case of pS1177, the salt bridge formed in the flavodoxin-binding domain (R630 formed salt bridge interactions with D668 and D637) (Table S2 of the ESM). It should be noted that S1177D and S633A formed more of the complex salt bridges than the native and other forms did (Table S2 of the ESM). On the other hand, S633D and S615D only participated in simple salt bridges (Table S2 of the ESM).

Intermolecular interactions of eNOS–Akt complexes

The phosphorylation of eNOS by Akt is a Ca^{2+}-independent regulatory mechanism for activating eNOS. To evaluate the strength of the Akt–eNOS association, the binding interaction of the eNOS–Akt complex was examined in the native, phosphorylated, phosphomimetic, and phosphomutant eNOSs. The three-dimensional structure of the $eNOS_{red}$ domain is required to elucidate the mechanism of the enzyme–substrate interaction. In the absence of the complete crystal structure, homology modeling and MD simulations were performed to obtain the energy-minimized structure of Akt (Figs. S3 and S4). The energy-optimized structures of native, phosphorylated, phosphomimetic, and phosphomutant $eNOS_{red}$s and Akt

Table 1 Summary of the intramolecular hydrogen bonds that are formed among the residues of the eNOS_ pS1177 and eNOSs_ S1177D

eNOS	Donor	Acceptor	Donor–acceptor distance (Å)	Hydrogen–acceptor distance (Å)
pS1177	A1142[N]	S615[O]	3.18	2.46
	N614[N]	S633[O]	3.42	2.48
	N614[ND2]	S633[OG]	2.93	2.12
S1177D	S615[N]	I611[O]	3.18	2.18
	S617[OG]	S633[OG]	3.03	2.30
	Y962[OH]	D1177[OD1]	2.86	1.96
	T1170[OG1]	D1177[OD2]	2.78	1.82
	D1177[N]	S1171[OG]	2.88	1.96
	S1171 [OG]	D1177[OD2]	3.10	2.17

were subjected to protein–protein docking, and the protein complex with the lowest RMSD was selected for further analysis (Table 2). Further, we examined the intermolecular interactions of the following docked complexes: eNOS–Akt, eNOS_pS615–Akt, eNOS_pS633–Akt, eNOS_pS1177–Akt, eNOS_S615D–Akt, eNOS_S633D–Akt, eNOS_S1177D–Akt, eNOS_S615A–Akt, eNOS_S633A–Akt, and eNOS_S1177A–Akt. The strongest association was observed for eNOS_pS1177 with Akt, which underscores the role of pS1177 in increasing the enzymatic activity. Further, the eNOS_pS615–Akt complex showed a higher number of H-bonds than the eNOS_pS633–Akt complex. Moreover, it was also noted that most of the hydrogen bonds formed in the FMN- and FAD-binding regions of eNOS (Table S3 of the ESM). The binding interfaces of the native eNOS–Akt, eNOS_S615D–Akt, and eNOS_S1177D–Akt complexes tend to form more salt bridges, contributing to electrostatic interactions, with a distance cutoff of 4 Å between charged residue side chains. More details of the intermolecular interactions in these and other complexes are provided in Tables S3 and S4 of the ESM.

Discussion

In endothelial cells, multiple and distinct control mechanisms regulate the enzymatic activity of eNOS to facilitate optimal stimulation of NO production. Post-translational modification (i.e., phosphorylation) is one control mechanism that is employed to regulate eNOS enzymatic activity [22]. In the present study, which focused on the eNOS reductase domain, the structural features of native, phosphorylated, phosphomimetic, and phosphomutant states of eNOS were examined by determining the conformations and dynamics of proteins as well as their interactions.

In the absence of experimentally derived structural details for the eNOS reductase domain, a 3D structure was derived by homology modeling with multiple templates, which was further analyzed to explore the structural features that may influence the enzymatic activity of eNOS. The generated 3D structure possesses all of the required stereochemical properties and hence represents a good-quality model.

In order to discern the role of phosphorylation-induced conformational dynamics in the regulatory mechanism, MD simulations were performed with phosphorylated serine residues. Significantly larger fluctuations were observed in the phosphorylated eNOS compared to the native eNOS. Experimental data suggests that phosphorylating S633 and S1177 stimulates eNOS activity, leading to increased NO production [43]. The simulation results revealed that residues in the flavodoxin-, FAD-, and NAD-binding domains were more flexible in the pS633 eNOS than in the pS1177 eNOS. On the other hand, the pS633 eNOS exhibited the greatest

Table 2 HADDOCK-derived energy parameters, RMSD values, surface areas, and scores for docked complexes of various forms of eNOS with Akt

	eNOS_Akt	pS1177_Akt	pS633_Akt	pS615_Akt	S1177D_Akt	S633D_Akt	S615D_Akt	S1177A_Akt	S633A_Akt	S615A_Akt
Haddock score	69.7±16.3	53.6±9.5	197.9±18.6	44.4±15.0	13.7±5.3	55.7±10.3	28.4±27.1	77.5±35.9	101.6±35.1	81.7±26.7
RMSD	1.3±1.7	0.8±0.6	18.1±0.6	0.6±0.4	0.6±0.1	5.4±0.2	0.5±0.3	2.0±1.2	6.6. ± 0.6	1.8±2.3
van der Waals Energy (kcal mol^{-1})	−91.1±11.6	−126.8±8.6	−91.3±7.5	−109.8±12.5	−103.0±11.9	−132.4±9.6	−108.0±7.2	−104.0±19.2	−78.2±4.8	−95.8±11.6
Electrostatic energy (kcal mol^{-1})	−591.8±56.8	−646.9±38.4	−356.4±19.2	−530.1±33.7	−934.8±61.2	−482.7±28.4	−756.4±45.9	−617.9±98.9	−541.3±152.8	558.1±55.9
Desolvation energy (kcal mol^{-1})	159.4±9.3	164.5±11.2	170.5±12.1	168.7±18.7	175.7±11.3	157.3±12.2	180.8±7.6	172.9±15.4	148.3±10.3	162.8±9.9
Restraints violation energy (kcal mol^{-1})	1197.7±28.18	1453.0±140.65	1900.3±108.18	914.9±90.54	1279.2±202.8	1273.8±72.7	1069.1±196.4	1322.9±157.5	1397.6±163.5	1263.7±67.8
Buried surface area ($Å^2$)	3083.1±131.4	4191.9±90.3	2515.0±95.7	3464.4±42.1	3942.8±195.7	4203.7±152.6	4016.1±348.6	3703.9±338.2	3415.7±453.8	3480.7±249.2
Z score	−1.4	−2.7	0.9	−1.7	−1.5	−1.0	−1.4	0.4	0.6	−0.9

flexibility at S1177, showing the relationship between the major phosphorylation residues observed experimentally [40].

Experimentally, the role of protein phosphorylation at a specific site is discerned by performing loss of function (serine to alanine) and gain of function (serine to aspartate) mutant studies. Therefore, we investigated the effects of phosphorylating serine residues (S615, S633, and S1177) in the $eNOS_{red}$ domain [18, 40]. It has been reported that different pathways lead to the phosphorylation of eNOS at specific residues. Once phosphorylated at a specific residue, structural modulation can be expected to regulate subsequent phosphorylation/dephosphorylation at other residues. In the in silico loss of function and gain of function studies performed in the present work, the associated structural dynamics were elucidated.

RMSD analysis suggested that there are marginal but important structural differences among the phosphomimetic eNOSs. Data on the flexibility of the phosphorylated residues exhibited some interesting features. The maximum and minimum RMSFs of 1.3 Å and 0.69 Å were observed for S1177 upon substitution of S633A and S633D. From the perspective of phosphomimetic proteins, the above finding suggests that S633 is a plausible candidate modulator of S1177. Though experimental studies of biochemical pathways utilize phosphomimetic proteins as cellular models, it is important to note that the simulation results for phosphorylated serine, which is an accurate model system, do not support this observation.

Though all of the serine residues involved in phosphorylation are localized in the loop region, it should be emphasized that S1177 exhibited reduced residue flexibility. At the same time, in the phosphomimetic and phosphorylated forms, S1177 contributes the greatest number of hydrogen bonds and salt bridges, ensuring the stability of the structure. These results corroborate the notion that S1177D and pS1177 are crucial to the efficient activation of eNOS [21].

Upon comparing the distinct forms of eNOS, it was found that S633 is the most solvent accessible of the phosphorylation residues. Experimental observations reported in the literature suggest that S633 functions as a stimulatory phosphorylation site which is stimulated in response to shear stress [43]. Furthermore, PKA phosphorylation at S633 in response to shear stress has been shown to increase NO production without requiring an increase in intracellular Ca^{2+} [23]. Therefore, it can be inferred that the high residue flexibility and solvent-accessible nature of S633 could make it a potential phosphorylation site that is stimulated by mechanical shear stress.

In addition, we studied the interaction of eNOS with Akt, which causes direct phosphorylation of eNOS, leading to Ca^{2+}-independent activation with increased NO production [44]. It should be emphasized that Akt phosphorylates eNOS at S615 and S1177 to regulate stimulus-mediated survival signals in endothelial cells [45, 21]. Computational analysis of the docked complex eNOS–Akt reveals that, in addition to S1177D and S615D, dephosphorylation at S633 enhances the binding of Akt to eNOS, leading to increased H-bond and salt-bridge formation. Further, two complexes, namely eNOS_pS615–Akt and eNOS_pS1177–Akt, showed a high tendency to bind with Akt. These findings suggest that phosphorylation, in addition to increasing the flexibility of residues, also modulates the network of hydrogen bonds and salt bridges. Note that, despite the marginal structural differences observed between phosphorylated and phosphomimetic eNOSs in the simulation, the phosphomimetic eNOS show significant differences in its H-bond interactions, which may have implications in protein–protein associations relevant to signaling events. This underscores the need to validate the experimental observations of specific molecular interactions using simulation data for phosphorylated and phosphomimetic proteins.

Even though our data could not directly relate phosphorylation-induced eNOS activity to NO release, since it is complicated by the presence of additional regulatory factors including hsp90 and caveolin [46], it should be emphasized that most of the inter- and intramolecular interactions of eNOS occur within the FMN- and FAD-binding domains. Therefore, the cofactor-binding region of eNOS may play a key role in the precise control of phosphorylation residues in the regulation of endothelial NO synthesis. In the absence of more structural evidence for the interaction between eNOS and Akt, our simulations highlighted the molecular interactions of distinct forms, which provide insight into the residues that are potentially useful for modulating the activity of eNOS. Thus, the subtle relationship between the eNOS and Akt interactions has been unraveled. Further, it should be stressed that the potential binding interactions observed in the study are not necessarily predictive of whether efficient phosphate transfer will occur. In summary, our results elucidate the effects of phosphorylation-dependent changes in eNOS through structural changes and protein–protein interactions, which could lead to a better understanding of NO production in endothelial cells.

Conclusion

The simulation study reported here investigated the conformational changes associated with distinct eNOS. The outcome of this study supports some of the key experimental observations reported in the literature on the role of phosphorylation in eNOS regulation. The salient feature of this study is that the highly flexible and solvent-exposed S633 was found in its phosphomimetic and phosphomutant states to modulate the flexibility of S1177, suggesting that S633 is a modulator of phosphorylation at other sites. However, it should be emphasized that a comparison of phosphorylated (pS633) and native eNOSs suggests that S633 does not qualify as a modulator.

This finding highlights the need to correlate the experimental dissection of biochemical pathways, as performed on mimetic and mutant states of proteins, with accurate model simulations. Further, the present discussion pertains to the reductase domain. This model could be extended further by combining the oxygenase and reductase domains along with the cofactors and prosthetic groups, thus permitting a comprehensive simulation study of the oxidation–reduction activities of eNOS. In summary, investigating the mechanism of phosphorylation—which occurs via multiple pathways and culminates in the tight regulation of eNOS, facilitating the efficient release of NO—could shed light on some subtle variations that ultimately drive the activation process. In brief, study that correlates structural dynamics with molecular interactions could extend our understanding of the structure–flexibility–activity of eNOS.

Acknowledgments We acknowledge Dr. M. Suresh Kumar for critical suggestions and encouragement and Mr. Om Prakash Sharma for help with the software. The Centre for Green Energy Technology is acknowledged for allowing N.T.D. to use their facilities as a visiting scholar. This work was partially supported by the Department of Biotechnology, Government of India, grant no. BT/PR7628/BRB/2006.

References

1. Moncada S, Higgs EA (2006) Nitric oxide and the vascular endothelium. Handb Exp Pharmacol 176:213–254
2. Förstermann U, Pollock JS, Nakane M (1993) Nitric oxide synthases in the cardiovascular system. Trends Cardiovasc Med 3:104–110
3. Bredt DS, Hwang PM, Snyder SH (1990) Localization of nitric oxide synthase indicating a neural role for nitric oxide. Nature 347:768–770
4. Wright CD, Mülsch A, Busse R, Osswald H (1989) Generation of nitric oxide by human neutrophils. Biochem Biophys Res Commun 160:813–819
5. Janssens SP, Shimouchi A, Quertermous T, Bloch DB, Bloch KD (1992) Cloning and expression of a cDNA encoding human endothelium-derived relaxing factor/nitric oxide synthase. J Biol Chem 267:14519–14522
6. Alderton WK, Cooper CE, Knowles RG (2001) Nitric oxide synthases: structure, function and inhibition. Biochem J 357:593–615
7. Cines DB, Pollak ES, Buck CA, Loscalzo J, Zimmerman GA et al (1998) Endothelial cells in physiology and in the pathophysiology of vascular disorders. Blood 91:3527–3561
8. Cooke JP, Dzau VJ (1997) Nitric oxide synthase: role in the genesis of vascular disease. Annu Rev Med 48:489–509
9. Du M, Yeh HC, Berka V, Wang LH, Tsai A (2003) Redox properties of human endothelial nitric-oxide synthase oxygenase and reductase domains purified from yeast expression system. J Biol Chem 278: 6002–6011
10. Martásek P, Miller RT, Liu Q, Roman LJ, Salerno JC et al (1998) The C331A mutant of neuronal nitric-oxide synthase is defective in arginine binding. J Biol Chem 273:34799–34805
11. Sessa WC, Harrison JK, Barber CM, Zeng D, Durieux ME et al (1992) Molecular cloning and expression of a cDNA encoding endothelial cell nitric oxide synthase. J Biol Chem 267:15274–15276
12. Feron O, Belhassen L, Kobzik L, Smith TW, Kelly RA et al (1996) Endothelial nitric oxide synthase targeting to caveolae. Specific interactions with caveolin isoforms in cardiac myocytes and endothelial cells. J Biol Chem 271:22810–22814
13. Mount PF, Kemp BE, Power DA (2007) Regulation of endothelial and myocardial NO synthesis by multi-site eNOS phosphorylation. J Mol Cell Cardiol 42:271–279
14. McCabe TJ, Fulton D, Roman LJ, Sessa WC (2000) Enhanced electron flux and reduced calmodulin dissociation may explain "calcium-independent" eNOS activation by phosphorylation. J Biol Chem 275:6123–6128
15. Morales-Ruiz M, Fulton D, Sowa G, Languino LR, Fujio Y et al (2000) Vascular endothelial growth factor-stimulated actin reorganization and migration of endothelial cells is regulated via the serine/threonine kinase Akt. Circ Res 86:892–896
16. Michell BJ, Z-p C, Tiganis T, Stapleton D, Katsis F et al (2001) Coordinated control of endothelial nitric-oxide synthase phosphorylation by protein kinase C and the cAMP-dependent protein kinase. J Biol Chem 276:17625–17628
17. Lane P, Gross SS (2002) Disabling a C-terminal autoinhibitory control element in endothelial nitric-oxide synthase by phosphorylation provides a molecular explanation for activation of vascular NO synthesis by diverse physiological stimuli. J Biol Chem 277:19087–19094
18. Boo YC, Sorescu G, Boyd N, Shiojima I, Walsh K et al (2002) Shear stress stimulates phosphorylation of endothelial nitric-oxide synthase at Ser1179 by Akt-independent mechanisms: role of protein kinase A. J Biol Chem 277:3388–3396
19. Harris MB, Ju H, Venema VJ, Liang H, Zou R et al (2001) Reciprocal phosphorylation and regulation of endothelial nitric-oxide synthase in response to bradykinin stimulation. J Biol Chem 276:16587–16591
20. Montagnani M, Chen H, Barr VA, Quon MJ (2001) Insulin-stimulated activation of eNOS is independent of Ca^{2+} but requires phosphorylation by Akt at Ser (1179). J Biol Chem 276:30392–30398
21. Michell BJ, Griffiths JE, Mitchelhill KI, Rodriguez-Crespo I, Tiganis T et al (1999) The Akt kinase signals directly to endothelial nitric oxide synthase. Curr Biol 9:845–848
22. Rafikov R, Fonseca FV, Kumar S, Pardo D, Darragh C et al (2011) eNOS activation and NO function: structural motifs responsible for the posttranslational control of endothelial nitric oxide synthase activity. J Endocrinol 210:271–284
23. Boo YC, Sorescu GP, Bauer PM, Fulton D, Kemp BE et al (2003) Endothelial NO synthase phosphorylated at SER635 produces NO without requiring intracellular calcium increase. Free Radic Biol Med 35:729–741
24. Fischmann TO, Hruza A, Niu XD, Fossetta JD, Lunn CA et al (1999) Structural characterization of nitric oxide synthase isoforms reveals striking active-site conservation. Nat Struct Biol 6:233–242
25. Garcin ED, Bruns CM, Lloyd SJ, Hosfield DJ, Tiso M et al (2004) Structural basis for isozyme-specific regulation of electron transfer in nitric-oxide synthase. J Biol Chem 279:37918–37927
26. Atochin DN, Wang A, Liu VW, Critchlow JD, Dantas AP et al (2007) The phosphorylation state of eNOS modulates vascular reactivity and outcome of cerebral ischemia in vivo. J Clin Invest 117:1961–1967
27. Eswar N, Webb B, Marti-Renom MA, Madhusudhan MS, Eramian D et al. (2006) Comparative protein structure modeling using Modeller. Curr Protocol Bioinform Unit 5.6. Wiley, Hoboken
28. Laskowski RA, MacArthur MW, Moss DS, Thornton JM (1993) PROCHECK: a program to check the stereochemical quality of protein structures. J Appl Cryst 26:283–291
29. Lüthy R, Bowie JU, Eisenberg D (1992) Assessment of protein models with three-dimensional profiles. Nature 356:83–85
30. Colovos C, Yeates TO (1993) Verification of protein structures: patterns of nonbonded atomic interactions. Protein Sci 2:1511–1519

31. Van Der Spoel D, Lindahl E, Hess B, Groenhof G, Mark AE et al (2005) GROMACS: fast, flexible, and free. J Comput Chem 26: 1701–1718
32. Margreitter C, Petrov D, Zagrovic B (2013) Vienna-PTM web server: a toolkit for MD simulations of protein post-translational modifications. Nucleic Acids Res W422–6
33. Martonák R, Laio A, Parrinello M (2003) Predicting crystal structures: the Parrinello–Rahman method revisited. Phys Rev Lett 90:075503
34. Cuendet MA, van Gunsteren WF (2007) On the calculation of velocity-dependent properties in molecular dynamics simulations using the leapfrog integration algorithm. J Chem Phys 127:184102
35. Ahmad S, Gromiha M, Fawareh H, Sarai A (2004) ASAView: database and tool for solvent accessibility representation in proteins. BMC Bioinform 1:5–51
36. de Vries SJ, van Dijk M, Bonvin AM (2010) The HADDOCK web server for data-driven biomolecular docking. Nat Protoc 5:883–897
37. de Vries SJ, Bonvin AM (2011) CPORT: a consensus interface predictor and its performance in prediction-driven docking with HADDOCK. PLoS One 6:e17695
38. Costantini S, Colonna G, Facchiano AM (2008) ESBRI: a web server for evaluating salt bridges in proteins. Bioinformation 3:137–138
39. Tina KG, Bhadra R, Srinivasan N (2007) PIC: Protein Interactions Calculator. Nucleic Acids Res 35:W473–W476
40. Bauer PM, Fulton D, Boo YC, Sorescu GP, Kemp BE (2003) Compensatory phosphorylation and protein-protein interactions revealed by loss of function and gain of function mutants of multiple serine phosphorylation sites in endothelial nitric-oxide synthase. J Biol Chem 278:14841–14849
41. Chen Z-P, Mitchelhill KI, Michell BJ, Stapleton D, Rodriguez-Crespo I et al (1999) AMP-activated protein kinase phosphorylation of endothelial NO synthase. FEBS Lett 443:285–289
42. Fulton D, Gratton JP, Sessa WC (2001) Post-translational control of endothelial nitric oxide synthase: why isn't calcium/calmodulin enough? J Pharmacol Exp Ther 299:818–824
43. Chen Z, Peng IC, Sun W, Su MI, Hsu PH et al (2009) AMP-activated protein kinase functionally phosphorylates endothelial nitric oxide synthase Ser633. Circ Res 104:496–505
44. Dimmeler S, Fleming I, Fisslthaler B, Hermann C, Busse R et al (1999) Activation of nitric oxide synthase in endothelial cells by Akt-dependent phosphorylation. Nature 399:601–605
45. Fulton D, Gratton JP, McCabe TJ, Fontana J, Fujio Y et al (1999) Regulation of endothelium-derived nitric oxide production by the protein kinase Akt. Nature 399:597–601
46. Brouet A, Sonveaux P, Dessy C, Moniotte S, Balligand JL et al (2001) Hsp90 and caveolin are key targets for the proangiogenic nitric oxide-mediated effects of statins. Circ Res 89:866–873